

Mask-based Latent Reconstruction for Reinforcement Learning

Tao Yu ^{*1} Zhizheng Zhang ^{*2} Cuiling Lan ² Zhibo Chen ¹ Yan Lu ²

Abstract

For deep reinforcement learning (RL) from pixels, learning effective state representations is crucial for achieving high performance. However, in practice, limited experience and high-dimensional input prevent effective representation learning. To address this, motivated by the success of masked modeling in other research fields, we introduce mask-based reconstruction to promote state representation learning in RL. Specifically, we propose a simple yet effective self-supervised method, Mask-based Latent Reconstruction (MLR), to predict the complete state representations in the latent space from the observations with spatially and temporally masked pixels. MLR enables the better use of context information when learning state representations to make them more informative, which facilitates RL agent training. Extensive experiments show that our MLR significantly improves the sample efficiency in RL and outperforms the state-of-the-art sample-efficient RL methods on multiple continuous benchmark environments.

1. Introduction

Learning effective state representations is crucial for reinforcement learning (RL) from vision signals (where a sequence of images is the input to an RL network), such as DeepMind Control Suite (Tassa et al., 2018). Inspired by the success of masked pre-training in the fields of Neural Language Processing (NLP) (Devlin et al., 2018; Radford et al., 2018; 2019; Brown et al., 2020) and Computer Vision (CV) (Bao et al., 2021; He et al., 2021; Xie et al., 2021), we make the first endeavor to explore the idea of mask-based reconstruction in RL.

Masked pre-training aims to exploit the reconstruction of masked word embeddings or pixels to promote feature learn-

ing in NLP or CV. This is in fact not straightforwardly applicable for RL due to the following reasons. 1) RL agents learn from interactions with environments, where the experienced states vary as the policy network is updated. Intuitively, collecting additional rollouts for pre-training is often costly in the real-world applications. Besides, it is challenging to learn effective state representations without the awareness on the learned policy. 2) Vision signals are commonly of high information densities, which may contain distractions and redundancies for the policy learning. Thus, for RL, performing reconstruction in the original (pixel) space is not as necessary as it is in the CV or NLP domain.

Based on the analysis above, we study the masked modeling tailored to vision-based RL. We present Mask-based Latent Reconstruction (MLR), a simple yet effective self-supervised method, to better learn state representations in RL. Contrary to treating masked modeling as a pre-training task in the fields of CV and NLP, our proposed MLR is an auxiliary objective optimized together with the policy learning objectives. In this way, the coordination between representation learning and policy learning are considered within a joint training framework. Apart from this, another key difference compared to vision/language research is that we reconstruct masked pixels in the latent space instead of the input space, where we take the state representations (*i.e.*, features) inferred from original unmasked frames as the reconstruction targets. This effectively reduces unnecessary reconstruction relative to the pixel-level one, and further facilitates the coordination between representation learning and policy learning because the state representations are directly optimized.

Consecutive frames are highly correlated. In MLR, we exploit this property to enable the learned state representations to be more informative, predictive and consistent over both spatial and temporal dimensions. Specifically, we randomly mask a portion of space-time cubes in the input observation (*i.e.*, video clip) sequence and reconstruct the missing contents in the latent space. In this way, similar to the spatial reconstruction for images in (He et al., 2021; Xie et al., 2021), MLR enhances the awareness of the agents to the global context information of the entire input observations and promotes the state representations to be predictive in both spatial and temporal dimensions. The predictive global information is encouraged to be encoded into each

^{*}Equal contribution ¹University of Science and Technology of China ²Microsoft Research Asia. Correspondence to: Zhizheng Zhang <zhizzhang@microsoft.com>, Cuiling Lan <cuilan@microsoft.com>, Zhibo Chen <chenzhibo@ustc.edu.cn>.

frame-level state representation, which achieves better representation learning and further facilitates the policy learning.

Not only is an effective masked modeling method proposed, we also conduct a systematical empirical study for the practices of masking and reconstruction that are as applicable to RL as possible. First, we study the influence of masking strategies by comparing spatial masking, temporal masking and space-time masking. Second, we investigate the differences between masking and reconstructing in the pixel space and in the latent space. Finally, we study how to effectively add reconstruction supervisions in the latent space.

Our contributions are summarized below:

- We introduce the idea of enhancing representation learning by mask-based reconstruction to RL for improving the sample efficiency. We integrate the mask-based reconstruction into RL training with an auxiliary objective, obviating the need for collecting additional rollouts for pre-training and helping the coordination between representation learning and policy learning in RL.
- We propose Mask-based Latent Reconstruction (MLR), a self-supervised masked modeling method to improve the state representations for RL. Tailored to RL, we propose to randomly mask space-time cubes in the pixel space and reconstruct the missing content from the unmasked pixels in the latent space. This is demonstrated to be effective for improving the sample efficiency on multiple continuous benchmark environments.
- A systematical empirical study is conducted to investigate the good practices of masking and reconstructing operations in MLR for RL. This demonstrates the effectiveness of our proposed designs in MLR.

2. Related Work

2.1. Representation Learning for RL

Reinforcement learning from vision signals is of high practical values in real-world applications such as robotics, video game AI, *etc.* However, such high-dimensional observations may contain distractions or redundant information, imposing considerable challenges for RL agents to learn effective representations (Shelhamer et al., 2017). Many prior works address this challenge by taking advantages of self-supervised learning to promote the representation learning of the states in RL. A popular approach is to jointly learn policy learning objectives and auxiliary objectives such as pixel reconstruction (Shelhamer et al., 2017; Yarats et al., 2019), reward prediction (Jaderberg et al., 2016; Shelhamer et al., 2017), bisimulation (Zhang et al., 2021), dynamics prediction (Shelhamer et al., 2017; Guo et al., 2020; Lee et al., 2020a;b; Schwarzer et al., 2021a; Yu et al., 2021) and contrastive learning of instance discrimination (Laskin et al., 2020b) or (spatial -) temporal discrimination (Oord

et al., 2018; Anand et al., 2019; Stooke et al., 2020; Zhu et al., 2020; Mazoure et al., 2020). Another feasible way for acquiring good representations is to pre-train the state encoder to learn effective representations for the original observations before policy learning. It requires additional offline sample collection or early access to the environments (Hansen et al., 2019; Stooke et al., 2020; Liu & Abbeel, 2021b;a; Schwarzer et al., 2021b), which is not fully consistent with the principle of sample efficiency in practice. This work aims to design a more effective auxiliary task to improve the learned state representations towards sample-efficient RL.

2.2. Sample-Efficient Reinforcement Learning

Collecting rollouts from the interaction with the environment is commonly costly especially in the real world, leaving the sample efficiency of RL algorithms widely concerned. To improve the sample efficiency of vision-based RL (*i.e.*, RL from pixel observations), recent works design auxiliary tasks to explicitly improve the learned representations (Yarats et al., 2019; Laskin et al., 2020b; Lee et al., 2020a;b; Zhu et al., 2020; Liu et al., 2021; Schwarzer et al., 2021a; Ye et al., 2021; Yu et al., 2021), or adopt data augmentation techniques, such as random cropping or shifting, to improve the diversity of data used for training based on collected samples (Yarats et al., 2021; Laskin et al., 2020a). Besides, there are some model-based methods that learn (world) models in the pixel (Łukasz Kaiser et al., 2020) or latent space (Hafner et al., 2019; 2020a;b; Ye et al., 2021), and perform planning, imagination or policy learning based on the learned models. We focus on the auxiliary task line in this work.

2.3. Masked Language/Image Modeling

Masked Language Modeling (MLM) (Devlin et al., 2018) and its autoregressive variants (Radford et al., 2018; 2019; Brown et al., 2020) achieve significant success in the NLP field and produce impacts in other domains. MLM masks a portion of word tokens from the input sentence and trains the model to predict the masked tokens, which has been demonstrated generally effective in learning language representations for various downstream tasks. For computer vision (CV) tasks, similar to MLM, masked image modeling (MIM) learning representations for images/videos by pre-training the neural network to reconstruct masked pixels from visible ones. As an early exploration, the Context Encoder (Pathak et al., 2016) apply this idea to Convolutional Neural Network (CNN) model to train a CNN model with a masked region inpainting task. With the recent popularity of the transformer-based architectures, a series of works (Chen et al., 2020; Bao et al., 2021; He et al., 2021; Xie et al., 2021; Wei et al., 2021) dust off the idea of MIM and show impressive performance on learning representations for vision

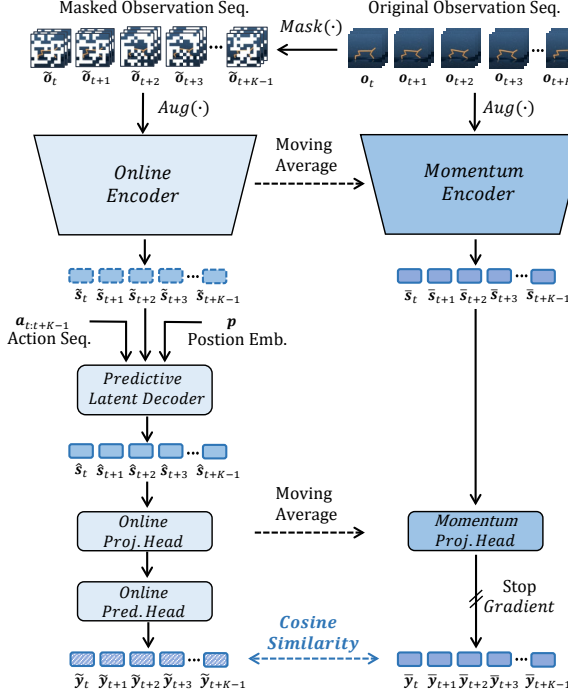


Figure 1. The framework of our method MLR. We perform a random spatial-temporal masking (*i.e.*, cube masking) on the sequence of consecutive observations in the pixel space. The masked observations are encoded to be the latent states with an online encoder. We further introduce a predictive latent decoder to decode/predict the latent states conditioned on the corresponding action sequence and a temporal positional embedding. Our method trains the networks to reconstruct the missing contents in an appropriate *latent* space using a cosine similarity based distance metric applied between the predicted features of the reconstructed states and the target features inferred from original observations by momentum networks.

tasks. Inspired by MLM and MIM, we explore the masked modeling for RL to exploit the high correlation in vision data to improve the awareness of agents to global-scope dynamics in learning state representations. Most importantly, *we propose to predict the masked contents in the latent space*, instead of the pixel space like aforementioned MIM works, which better coordinates the representation learning and the policy learning in RL.

3. Approach

3.1. Background

Vision-based RL aims to learn policies from interactions with the observations composed of pixels. The learning process corresponds to a Markov Decision Process (MDP) (Bellman, 1957; Kaelbling et al., 1998). Generally, at the timestep t , given the observation \mathbf{o}_t from the environment, the RL agent responds to this observation by taking an

action \mathbf{a}_t . When the environment receives \mathbf{a}_t , it will transfer \mathbf{o}_t to the next observation \mathbf{o}_{t+1} with a probability and return a reward r_t . Following the common practice in (Mnih et al., 2013), we encode several consecutive observations as a state (Bellman, 1957), which is a feature vector in the latent space. And the reward function and the transition dynamics can be written as $p = Pr(\mathbf{s}_{t+1}|\mathbf{s}_t, \mathbf{a}_t)$ and $r_t = r(\mathbf{s}_t, \mathbf{a}_t)$, respectively. The objective of RL is to learn a policy $\pi(\mathbf{a}_t|\mathbf{s}_t)$ that maximizes the cumulative discounted return $\mathbb{E}_\pi \sum_{t=1}^{\infty} \gamma^t r_t$, where γ is the discount factor.

Our proposed method is theoretically applicable for different RL algorithms. Following the common practices in prior sample-efficient RL studies (Yarats et al., 2019; Lee et al., 2020a; Laskin et al., 2020b; Yarats et al., 2021; Laskin et al., 2020a; Yu et al., 2021), we show its effectiveness based on a strong model-free RL agent Soft Actor Critic (SAC) in this paper. The detailed introduction of SAC can be found in Appendix A.

3.2. Mask-based Latent Reconstruction

Mask-based Latent Reconstruction (MLR) is an auxiliary objective to promote the learned representations from pixel-based observations in RL, towards sample-efficient RL. The core idea of MLR is to facilitate the state representation learning by reconstructing spatially and temporally masked pixels in the latent space. This mechanism enables the better use of context information when learning state representations, further enhancing the understanding of RL agents for vision signals. We illustrate the overall framework of MLR in Figure 1 and elaborate it below.

Framework. In MLR, as shown in Figure 1, we mask a portion of pixels in the input observation sequence along its spatial and temporal dimensions. We encode the masked sequence and the original sequence from observations to states with an encoder and a momentum encoder, respectively. Taking the states encoded from the original sequence as the target, we perform predictive reconstruction from the states corresponding to the masked sequence. We add reconstruction supervisions between prediction results and targets in the decoded latent space. The processes of *masking*, *encoding*, *decoding* and *reconstruction* are introduced in detail below.

(i) Masking. Given an observation sequence of K timesteps $\tau_K^o = \{\mathbf{o}_t, \mathbf{o}_{t+1}, \dots, \mathbf{o}_{t+K-1}\}$, with the shape of $H \times W \times K$, the frames in the observations are stacked to be a cuboid. As illustrated in Figure 2, we divide the cuboid into regular non-overlapping *cubes* with the shape of $h \times w \times k$. We then randomly mask a portion of cubes following a uniform distribution and obtain a masked observation sequence $\tilde{\tau}_K^o = \{\tilde{\mathbf{o}}_t, \tilde{\mathbf{o}}_{t+1}, \dots, \tilde{\mathbf{o}}_{t+K-1}\}$. Following (Yu et al., 2021), we perform stochastic image augmentation (*e.g.*, random crop and intensity) on each masked observation in $\tilde{\tau}_K^o$. The

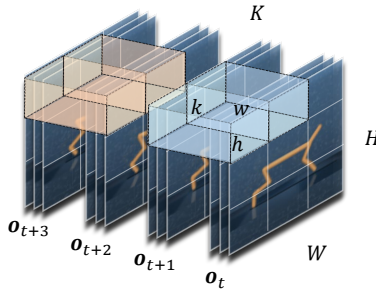


Figure 2. Illustration of our cube masking. We divide the input observation sequence to non-overlapping cubes ($h \times w \times k$). In this example, we have $h = \frac{1}{3}H$, $w = \frac{1}{3}W$ and $k = \frac{1}{2}K$ where the observation sequence has $K = 4$ timesteps and a spatial size of $H \times W$.

objective of MLR is to predict the state representations of unmasked observation sequence from the masked one in the latent space.

(ii) Encoding. We adopt two encoders to learn state representations from masked observations and original observations respectively. A regular CNN-based encoder f is used to encode each masked observation \tilde{o}_{t+i} into its corresponding state $\tilde{s}_{t+i} \in \mathbb{R}^d$. After the encoding, we obtain a sequence of the masked latent states $\tilde{\tau}_K^s = \{\tilde{s}_t, \tilde{s}_{t+1}, \dots, \tilde{s}_{t+K-1}\}$ for masked observations. The parameters of this encoder are updated based on gradient back-propagation in an end-to-end way. We thus call it “online” encoder. The state representations inferred from original observations are taken as the targets of subsequently described reconstruction. To make them more robust, inspired by (Laskin et al., 2020b; Schwarzer et al., 2021a; Yu et al., 2021), we exploit another encoder for the encoding of original observations. This encoder, called “Momentum Encoder” as in Figure 1, has the same architecture as the online encoder, and its parameters are updated by an exponential moving average (EMA) of the online encoder weights θ_f with the momentum coefficient $m \in [0, 1]$, as formulated below:

$$\bar{\theta}_f \leftarrow m\bar{\theta}_f + (1-m)\theta_f. \quad (1)$$

(iii) Decoding. Similar to the encoder designs in (He et al., 2021; Xie et al., 2021), the online encoder in our proposed MLR reconstructs the representations of masked contents based on visible ones in an *implicit* way. The predictive global information has been implicitly included into the outputs of the online encoder. To add the reconstruction loss between the state representations inferred from masked and original observations, we need compare them in a unified latent space. To this end, we leverage a Transformer-based latent decoder to refine the outputs of the online encoder via a global message passing where the actions and temporal information are exploited as the contexts. Through this

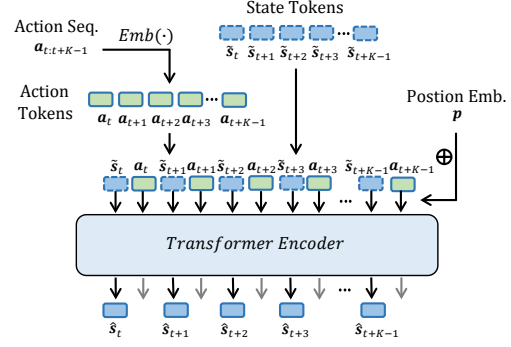


Figure 3. Illustration of predictive latent decoder.

process, the implicitly predicted information is “passed” to its corresponding states for adding reconstruction losses.

As shown in Figure 3, the input tokens of the latent decoder consist of both the masked state sequence $\tilde{\tau}_K^s$ (i.e., state tokens) and the corresponding action sequence $\tau_K^a = \{a_t, a_{t+1}, \dots, a_{t+K-1}\}$ (i.e., action tokens). Each action token is embedded as a feature vector with the same dimension as the stated token using an embedding layer. We integrate the relative positional embeddings $p \in \mathbb{R}^{K \times d}$ as in (Vaswani et al., 2017) to encode relative temporal positional information into both state and action tokens. Notably, the state and action token at the same timestep $t + i$ share the same positional embedding $p_{t+i} \in \mathbb{R}^d$. Thus, the inputs of latent decoder can be mathematically represented as:

$$\mathbf{x} = [\tilde{s}_t, a_t, \tilde{s}_{t+1}, a_{t+1}, \dots, \tilde{s}_{t+K-1}, a_{t+K-1}] + \mathbf{p}. \quad (2)$$

The input token sequence is passed through a Transformer encoder (Vaswani et al., 2017) consisting of L attention layers. Each layer is composed of a Multi-Headed Self-Attention (MSA) layer (Vaswani et al., 2017), a layer normalisation (LN) (Ba et al., 2016), and multilayer perceptron (MLP) blocks. The process can be described as follows:

$$\mathbf{z}^l = \text{MSA}(\text{LN}(\mathbf{x}^l)) + \mathbf{x}^l, \quad (3)$$

$$\mathbf{x}^{l+1} = \text{MLP}(\text{LN}(\mathbf{z}^l)) + \mathbf{z}^l. \quad (4)$$

The output tokens of the latent decoder, represented as $\hat{\tau}_K^s = \{\hat{s}_t, \hat{s}_{t+1}, \dots, \hat{s}_{t+K-1}\}$, are the predictive reconstruction results for the latent representations inferred from original observations. We elaborate the reconstruction loss between the prediction results and corresponding targets in the following.

(iv) Reconstruction loss. Motivated by the success of BYOL (Grill et al., 2020) in self-supervised learning, we use an asymmetric architecture for calculating the distance between the predicted/reconstructed latent states and the

target states, similar to (Schwarzer et al., 2021a; Yu et al., 2021). For the outputs of the latent decoder, we use a projection head g and a prediction head q to get the final prediction result $\hat{\mathbf{y}}_{t+i} = q(g(\hat{\mathbf{s}}_{t+i}))$ corresponding to \mathbf{s}_{t+i} . For the encoded results of original observations, we use a momentum updated projection head \bar{g} whose weights are updated with an EMA of the weights of the online projection head. These two projection heads have the same architectures. The outputs of the momentum projection head \bar{g} , *i.e.*, $\bar{\mathbf{y}}_{t+i} = \bar{g}(\bar{\mathbf{s}}_{t+i})$, are the final reconstruction targets. Here, we apply a stop-gradient operation as illustrated in Figure 1 to avoid model collapse, following (Grill et al., 2020).

The objective of MLR is to enforce the final prediction result $\hat{\mathbf{y}}_{t+i}$ to be as close as possible to its corresponding target $\bar{\mathbf{y}}_{t+i}$. To achieve this, we design the reconstruction loss in our proposed MLR by calculating the cosine similarity between $\hat{\mathbf{y}}_{t+i}$ and $\bar{\mathbf{y}}_{t+i}$, which can be formulated below:

$$\mathcal{L}_{mlr} = 2 - \frac{2}{K} \sum_{i=0}^{K-1} \frac{\hat{\mathbf{y}}_{t+i}}{\|\hat{\mathbf{y}}_{t+i}\|_2} \frac{\bar{\mathbf{y}}_{t+i}}{\|\bar{\mathbf{y}}_{t+i}\|_2}. \quad (5)$$

The loss \mathcal{L}_{mlr} is used to update the parameters of the online networks including encoder f , predictive latent decoder ϕ , projection head g and prediction head q . Through our proposed self-supervised auxiliary objective MLR, the learned state representations by the encoder will be more informative, thus can further facilitate the policy learning.

Objective. The proposed MLR is an auxiliary task, which is optimized together with the policy learning. Thus, the overall loss function \mathcal{L}_{total} for RL agent training is:

$$\mathcal{L}_{total} = \mathcal{L}_{rl} + \lambda \mathcal{L}_{mlr}, \quad (6)$$

where \mathcal{L}_{rl} and \mathcal{L}_{mlr} are the loss functions of the base RL agent (*e.g.*, SAC (Haarnoja et al., 2018)) and the proposed mask-based latent reconstruction, respectively. λ is a hyperparameter for balancing the two terms. Notably, the agent of vision-based RL commonly consists of two parts, *i.e.*, the (state) representation network (*i.e.*, encoder) and the policy learning network. The encoder of MLR is taken as the representation network to encode observations into the state representations for RL training, where the latent decoder is not adopted because unmasked observations are taken as the inputs. More details can be found in Appendix B.

4. Experiment

4.1. Setup

We evaluate our proposed MLR on the most popular vision-based continuous benchmark environments from DeepMind Control Suite (DMControl) (Tassa et al., 2018). Following the representative previous works (Laskin et al., 2020b; Yarats et al., 2021; Laskin et al., 2020a; Yu et al., 2021), we

choose six commonly used environments from DMControl, *i.e.*, *Finger, spin* (Fing.spin); *Cartpole, swingup* (Cart.swin); *Reacher, easy* (Reac.easy); *Cheetah, run* (Chee.run); *Walker, walk* (Walk.walk) and *Ball in cup, catch* (Ball.catch) for evaluation. We measure the performance of RL agents with the mean and median scores over 10 episodes at 100k and 500k environment steps as the test results, (referred to as **DMControl-100k** and **DMControl-500k** benchmarks), respectively. Concretely, DMControl-100k is used for measuring sample efficiency performance while DMControl-500k is used for measuring asymptotic performance. The score of each environment ranges from 0 to 1000 (Tassa et al., 2018). Unless otherwise specified, Soft Actor Critic (SAC) (Haarnoja et al., 2018) is taken as the base agent for effectiveness evaluation as it is in many previous work (Yarats et al., 2019; Lee et al., 2020a; Laskin et al., 2020b; Yarats et al., 2021; Laskin et al., 2020a; Yu et al., 2021).

In our experiments, we denote the base agent trained only by RL loss \mathcal{L}_{rl} (as in Equation 6) as *Baseline*, while denoting the model of applying our proposed MLR to the base agent as *MLR* for the brevity. As shown in Equation 6, we set a weight λ to balance \mathcal{L}_{rl} and \mathcal{L}_{mlr} so that the gradients of these two loss items lie in a similar range and empirically find $\lambda = 1$ works well. In MLR, by default, we set the length of a sampled trajectory K to 16, mask ratio η to 50% and the size of the masked cube ($h \times w \times k$) to $10 \times 10 \times 8$ (except for $k = 4$ in Cart.swin and Reac.easy due to their large motion range). More implementation details can be found in Appendix B.

4.2. Comparison with State-of-the-Arts

In this section, we compare our proposed *MLR* with the state-of-the-art (SOTA) sample-efficient RL methods proposed for continuous control, including PlaNet (Hafner et al., 2019), Dreamer (Hafner et al., 2020a), SAC+AE (Yarats et al., 2019), SLAC (Lee et al., 2020a), CURL (Laskin et al., 2020b), DrQ (Yarats et al., 2021) and PlayVirtual (Yu et al., 2021).

The comparison results are shown in Table 1, and all results are averaged over 10 repetitive experiments with different random seeds. From the results shown in Table 1, we can observe that: (i) The proposed MLR significantly improves *Baseline* in both sample efficiency (*i.e.*, DMControl-100k) and asymptotic performance (*i.e.*, DMControl-500k), and achieves consistent gains relative to *Baseline* across all environments. It is worthy to mention that, for the DMControl-100k, our proposed method outperforms *Baseline* by **25.3%** and **34.7%** in mean and median scores, respectively. This demonstrates the superiority of MLR in improving the sample efficiency of RL algorithms. (ii) The RL agent equipped with our proposed MLR outperforms most state-of-the-art methods on the DMControl-100k and DMControl-

Table 1. Comparison with the state-of-the-art methods and *Baseline* on DMControl-100k and DMControl-500k benchmarks. Scores (mean and standard deviation) on each environment are averaged over 10 random seeds. Our method augments *Baseline* with the proposed MLR objective (denoted as *MLR*).

100k Step Scores	PlaNet	Dreamer	SAC+AE	SLAC	CURL	DrQ	PlayVirtual	Baseline	MLR
Finger, spin	136 \pm 216	341 \pm 70	740 \pm 64	693 \pm 141	767 \pm 56	901 \pm 104	915 \pm 49	853 \pm 112	907 \pm 58
Cartpole, swingup	297 \pm 39	326 \pm 27	311 \pm 11	-	582 \pm 146	759 \pm 92	816 \pm 36	784 \pm 63	806 \pm 48
Reacher, easy	20 \pm 50	314 \pm 155	274 \pm 14	-	538 \pm 233	601 \pm 213	785 \pm 142	593 \pm 118	866 \pm 103
Cheetah, run	138 \pm 88	235 \pm 137	267 \pm 24	319 \pm 56	299 \pm 48	344 \pm 67	474 \pm 50	399 \pm 80	482 \pm 38
Walker, walk	224 \pm 48	277 \pm 12	394 \pm 22	361 \pm 73	403 \pm 24	612 \pm 164	460 \pm 173	424 \pm 281	643 \pm 114
Ball in cup, catch	0 \pm 0	246 \pm 174	391 \pm 82	512 \pm 110	769 \pm 43	913 \pm 53	926 \pm 31	648 \pm 287	933 \pm 16
Mean	135.8	289.8	396.2	471.3	559.7	688.3	729.3	616.8	772.8
Median	137.0	295.5	351.0	436.5	560.0	685.5	800.5	620.5	836.0
500k Step Scores									
Finger, spin	561 \pm 284	796 \pm 183	884 \pm 128	673 \pm 92	926 \pm 45	938 \pm 103	963 \pm 40	944 \pm 97	973 \pm 31
Cartpole, swingup	475 \pm 71	762 \pm 27	735 \pm 63	-	841 \pm 45	868 \pm 10	865 \pm 11	871 \pm 4	872 \pm 5
Reacher, easy	210 \pm 390	793 \pm 164	627 \pm 58	-	929 \pm 44	942 \pm 71	942 \pm 66	943 \pm 52	957 \pm 41
Cheetah, run	305 \pm 131	570 \pm 253	550 \pm 34	640 \pm 19	518 \pm 28	660 \pm 96	719 \pm 51	602 \pm 67	674 \pm 37
Walker, walk	351 \pm 58	897 \pm 49	847 \pm 48	842 \pm 51	902 \pm 43	921 \pm 4575	928 \pm 30	818 \pm 263	939 \pm 10
Ball in cup, catch	460 \pm 380	879 \pm 87	794 \pm 58	852 \pm 71	959 \pm 27	963 \pm 9	967 \pm 5	960 \pm 10	964 \pm 14
Mean	393.7	782.8	739.5	751.8	845.8	882.0	897.3	856.3	896.5
Median	405.5	794.5	764.5	757.5	914.0	929.5	935.0	907.0	948.0

500k. Specifically, our method surpasses the best previous method (*i.e.*, PlayVirtual) by 43.5 and 35.5 in mean and median scores respectively on DMControl-100k. Besides, our method delivers the best median score and reaches a comparable mean score with the strongest SOTA method on DMControl-500k. Note that PlayVirtual (Yu et al., 2021) generates virtual trajectories for RL training rather than designing auxiliary task to improve the representations like what we focus on in this paper. We are in fact complementary theoretically.

4.3. Ablation Study

Effectiveness evaluation. Besides the comparison with SOTA methods, we demonstrate the effectiveness of our proposed MLR by studying its improvements compared to our *Baseline*. The numerical results are presented in Table 1, while the curves of test performance during the training process are given in Figure 4. Both numerical results and test performance curves can demonstrate that our method obviously outperforms *Baseline* across different environments thanks to more informative representations learned by MLR.

Masking strategy. We compare three design choices of the masking operation: (i) *Spatial masking* (denoted as *MLR-S*): we randomly mask *patches* for each frame independently. (ii) *Temporal masking* (denoted as *MLR-T*): we divide the input observation sequence into multiple segments along the temporal dimension and mask out a portion of segments randomly. (Here, the segment length is set to be equal to the temporal length of cube, *i.e.*, k .) And (iii) *Spatial-temporal masking* (also referred to as “cube masking”): as aforementioned and illustrated in Figure 2, we rasterize the obser-

vation sequence into non-overlapping cubes and randomly mask a portion of them. Except for the differences described above, other configurations for masking remain the same as our proposed spatial-temporal (*i.e.*, cube) masking.

The experiment results of this ablation study on DMControl-100k are presented in Table 2. From such results, we have the following observations: (i) All three masking strategies (*i.e.*, *MLR-S*, *MLR-T* and *MLR*) achieve mean score improvements compared to *Baseline* by **18.5%**, **12.2%** and **25.0%**, respectively, and achieve median score improvements by **23.4%**, **25.0%** and **35.9%**, respectively. This demonstrates the effectiveness of the core idea of introducing mask-based reconstruction to improve the representation learning of RL. (ii) Spatial-temporal masking is the most effective strategy over these three design choices. This strategy matches better with the nature of video data due to its spatial-temporal continuity in masking. It encourages the state representations to be more predictive and consistent along the spatial and temporal dimensions, thus conducive to facilitating the policy learning in RL.

Reconstruction target. In masked language/image modeling, reconstruction/prediction is commonly performed in the original signal space, such as word embeddings or RGB pixels. To study the influence of reconstruction targets for the task of RL, we compare two different reconstruction spaces: (i) *Pixel space reconstruction* (denoted as *MLR-Pixel*): we predict the masked contents directly by reconstructing original pixels, like the practices in CV and NLP domains; (ii) *Latent space reconstruction* (*i.e.*, *MLR*): we reconstruct the state representations (*i.e.*, features) of original observations from masked observations, as we proposed in MLR. Table 3 shows the comparison results. The reconstruction in the

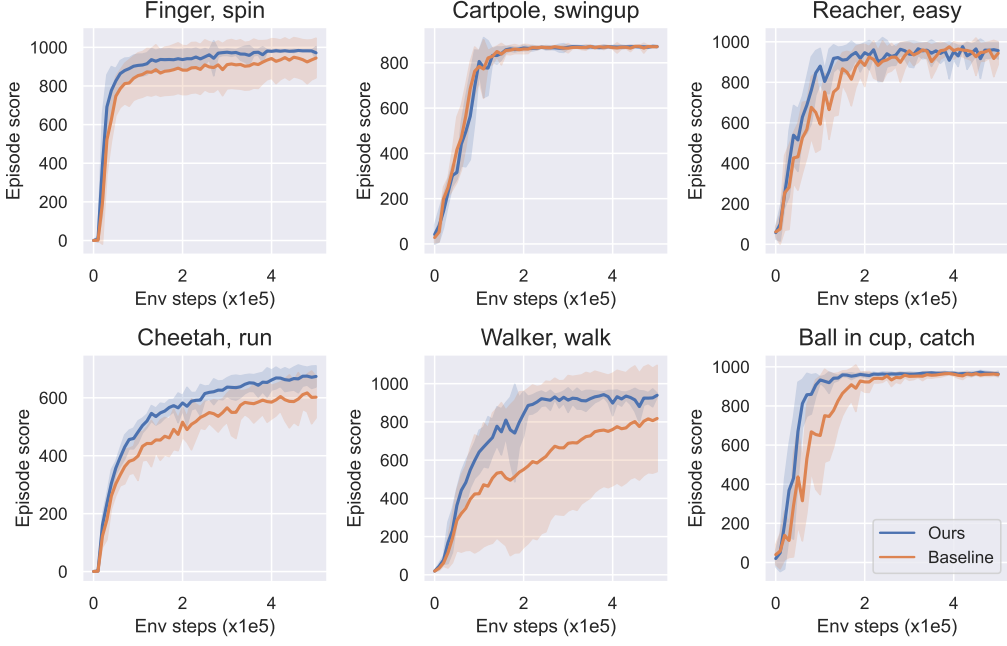


Figure 4. Test performance during the training period (500k environment steps). Lines denote the mean scores over 10 random seeds, and the shadows are the corresponding standard deviations. In most environments on DMControl, our results (blue lines) are consistently better than *Baseline* (orange lines).

Table 2. Ablation study of masking strategy on DMControl-100k benchmark. We compare three masking strategies: spatial masking (*MLR-S*), temporal masking (*MLR-T*) and spatial-temporal masking (*MLR*). The results are averaged over 5 random seeds.

Env.	Baseline	MLR-S	MLR-T	MLR
Fing.spin	822 ± 146	919 ± 55	787 ± 139	907 ± 69
Cart.swin	782 ± 74	665 ± 118	829 ± 33	791 ± 50
Reac.easy	557 ± 137	848 ± 82	745 ± 84	875 ± 92
Chee.run	438 ± 33	449 ± 46	443 ± 43	495 ± 13
Walk.walk	414 ± 310	556 ± 189	393 ± 202	597 ± 102
Ball.catch	669 ± 310	927 ± 6	934 ± 29	939 ± 9
Mean	613.7	727.3	688.5	767.3
Median	613.0	756.5	766.0	833.0

Table 3. Ablation study of reconstruction target on DMControl-100k benchmark. We compare two reconstruction targets, original pixels (denoted as *MLR-Pixel*) and momentum projections in the latent space (*i.e.*, *MLR*). We run each models for 5 random seeds.

Env.	Baseline	MLR-Pixel	MLR
Fing.spin	822 ± 146	782 ± 95	907 ± 69
Cart.swin	782 ± 74	803 ± 91	791 ± 50
Reac.easy	557 ± 137	787 ± 136	875 ± 92
Chee.run	438 ± 33	346 ± 84	495 ± 13
Walk.walk	414 ± 310	490 ± 216	597 ± 102
Ball.catch	669 ± 310	675 ± 292	939 ± 9
Mean	613.7	647.2	767.3
Median	613.0	728.5	833.0

latent space is superior to that in the pixel space in improving the sample efficiency in RL. As discussed in preceding sections, vision data might contain distractions and redundancies for the policy learning in RL, leaving the pixel-level reconstruction unnecessary. Besides, latent space reconstruction is more conducive to the coordination between the representation learning and the policy learning in RL, because the state representations are directly optimized.

Mask ratio. In recent works of masked image modeling (MIM) (He et al., 2021; Xie et al., 2021), the mask ratio is found crucial for the final performance. We study the influences of different masking ratios for sample efficiency in Figure 5, and find that the ratio of 50% is an appropriate choice for our proposed *MLR*. An over-small value of this

ratio could not eliminate redundancy, and make the objective easy to be reached by extrapolation from neighboring contents which is free of capturing and understanding semantics from vision signals. An over-large value leaves too few contexts for achieving the reconstruction goal. As discussed in (He et al., 2021; Xie et al., 2021), the choice of this ratio varies for different modalities and depends on the information density.

Decoder depth. We analyze the influence of using Transformer-based latent decoders of different depths. As the experimental results shown in Table 5, generally, deeper latent decoders lead to worse sample efficiency with lower mean and median scores. Notably, compared to the encoder (4.04M parameters), our decoder is lightweight (40.8K pa-

Table 4. Ablation studies on action token, masking features and momentum decoder. *MLR w.o. ActTok* denotes removing the action tokens in the input tokens of the predictive latent decoder. *MLR-F* indicates performing masking on convolutional feature maps. And *MLR-MoDec* indicates adding a momentum predictive latent decoder in the target networks. We run each models on DMControl-100k benchmark for 3 random seeds.

DMControl-100k	Baseline	MLR w.o. ActTok	MLR-F	MLR-MoDec	MLR
Finger, spin	841 \pm 150	843 \pm 34	845 \pm 137	905 \pm 67	904 \pm 70
Cartpole, swingup	785 \pm 72	822 \pm 8	807 \pm 30	779 \pm 75	808 \pm 40
Reacher, easy	631 \pm 55	840 \pm 58	828 \pm 171	808 \pm 57	880 \pm 82
Cheetah, run	431 \pm 31	403 \pm 82	469 \pm 49	472 \pm 178	487 \pm 9
Walker, walk	436 \pm 277	470 \pm 217	668 \pm 46	587 \pm 212	616 \pm 87
Ball in cup, catch	609 \pm 320	818 \pm 141	804 \pm 150	829 \pm 122	932 \pm 3
Mean		622.2	699.3	736.8	771.2
Median		620.0	820.0	805.5	844.0

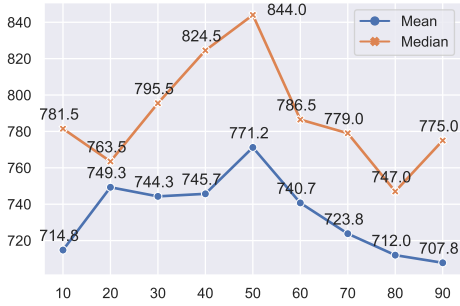


Figure 5. Ablation study of mask ratio. We run each model for 3 random seeds and report the average results.

Table 5. Ablation study of predictive latent decoder depth. We run each model on DMControl-100k benchmark for 5 random seeds. We report number of parameters, mean score and median score.

Layers	Param.	Mean Score	Median Score
1	20.4K	726.8	719.0
2	40.8K	767.3	833.0
4	81.6K	766.2	789.5
8	163.2K	728.3	763.5

rameters). Similar to the designs in (He et al., 2021; Xie et al., 2021), it is appropriate to use a lightweight decoder in MLR, because we actually expect the predicting masked information to be mainly completed by the encoder instead of the decoder. Note that the state representations inferred by the encoder are the ones adopted for the policy learning in RL.

Action token. We study the contributions of action tokens used for the latent decoder as illustrated in Figure 1 by discarding it from our proposed framework. The results are given in Table 4. Intuitively, prediction only from vision signals is of more or less ambiguity. Exploiting action tokens benefits reducing such ambiguity so that the gradients of less uncertainty can be obtained for updating the encoder.

Masking features. We compare ‘‘masking pixels’’ and

‘‘masking features’’ in Table 4. Masking features (denoted by *MLR-F*) does not perform equally well compared to masking pixels as proposed in MLR, but it still achieves significant improvements to *Baseline*.

Why not use a latent decoder for targets? We have also attempted to add a momentum updated latent decoder for the target states \bar{s}_{t+i} as illustrated in Figure 1. The results in Table 4 show that adding the momentum decoder leads to performance drops. This is because there is no information prediction for the state representation learning from the original observation sequence without masking. Thus, we do not need to refine the implicitly predicted information like that in the outputs \hat{s}_{t+i} of the online encoder.

Cube size and sequence length. These two factors can be viewed as hyperparameters. Their corresponding experimental analysis and results are in the Appendix C.

5. Conclusion

In this work, we make the first effort to introduce the popular mask-based reconstruction to RL for facilitating the policy learning by improving the learned state representations. We propose MLR, a simple yet effective self-supervised auxiliary objective to reconstruct the masked contents in the latent space. In this way, the learned state representations are encouraged to include richer and more informative features. Extensive experiments show that MLR achieves the state-of-the-art performance on DeepMind Control benchmarks and demonstrate its effectiveness. We conduct detailed ablation study for the proposed designs in MLR and analyze their differences from that in NLP and CV domains. We hope our proposed method can inspire further research for vision-based RL from the perspective of improving the representation learning. Moreover, the concept of the masked latent reconstruction is also worthy of being explored and extended in the fields of computer vision and neural language processing. We are looking forward to seeing more mutual promotion between different research fields.

References

Anand, A., Racah, E., Ozair, S., Bengio, Y., Côté, M.-A., and Hjelm, R. D. Unsupervised state representation learning in atari. In *Advances in Neural Information Processing Systems*, 2019.

Ba, J. L., Kiros, J. R., and Hinton, G. E. Layer normalization. *arXiv preprint arXiv:1607.06450*, 2016.

Bao, H., Dong, L., and Wei, F. Beit: Bert pre-training of image transformers. *arXiv preprint arXiv:2106.08254*, 2021.

Bellman, R. A markovian decision process. *Journal of mathematics and mechanics*, 6(5):679–684, 1957.

Brown, T. B., Mann, B., Ryder, N., Subbiah, M., Kaplan, J., Dhariwal, P., Neelakantan, A., Shyam, P., Sastry, G., Askell, A., et al. Language models are few-shot learners. *arXiv preprint arXiv:2005.14165*, 2020.

Chen, M., Radford, A., Child, R., Wu, J., Jun, H., Luan, D., and Sutskever, I. Generative pretraining from pixels. In *International Conference on Machine Learning*, pp. 1691–1703. PMLR, 2020.

Devlin, J., Chang, M.-W., Lee, K., and Toutanova, K. Bert: Pre-training of deep bidirectional transformers for language understanding. *arXiv preprint arXiv:1810.04805*, 2018.

Grill, J.-B., Strub, F., Altché, F., Tallec, C., Richemond, P., Buchatskaya, E., Doersch, C., Avila Pires, B., Guo, Z., Gheshlaghi Azar, M., Piot, B., kavukcuoglu, k., Munos, R., and Valko, M. Bootstrap your own latent - a new approach to self-supervised learning. In *Advances in Neural Information Processing Systems*, 2020.

Guo, Z. D., Pires, B. A., Piot, B., Grill, J.-B., Altché, F., Munos, R., and Azar, M. G. Bootstrap latent-predictive representations for multitask reinforcement learning. In *International Conference on Machine Learning*, pp. 3875–3886. PMLR, 2020.

Haarnoja, T., Zhou, A., Hartikainen, K., Tucker, G., Ha, S., Tan, J., Kumar, V., Zhu, H., Gupta, A., Abbeel, P., et al. Soft actor-critic algorithms and applications. *arXiv preprint arXiv:1812.05905*, 2018.

Hafner, D., Lillicrap, T., Fischer, I., Villegas, R., Ha, D., Lee, H., and Davidson, J. Learning latent dynamics for planning from pixels. In *International Conference on Machine Learning*, pp. 2555–2565. PMLR, 2019.

Hafner, D., Lillicrap, T., Ba, J., and Norouzi, M. Dream to control: Learning behaviors by latent imagination. In *International Conference on Learning Representations*, 2020a.

Hafner, D., Lillicrap, T., Norouzi, M., and Ba, J. Mastering atari with discrete world models. *arXiv preprint arXiv:2010.02193*, 2020b.

Hansen, S., Dabney, W., Barreto, A., Van de Wiele, T., Warde-Farley, D., and Mnih, V. Fast task inference with variational intrinsic successor features. *arXiv preprint arXiv:1906.05030*, 2019.

He, K., Chen, X., Xie, S., Li, Y., Dollár, P., and Girshick, R. Masked autoencoders are scalable vision learners. *arXiv preprint arXiv:2111.06377*, 2021.

Jaderberg, M., Mnih, V., Czarnecki, W. M., Schaul, T., Leibo, J. Z., Silver, D., and Kavukcuoglu, K. Reinforcement learning with unsupervised auxiliary tasks. *arXiv preprint arXiv:1611.05397*, 2016.

Kaelbling, L. P., Littman, M. L., and Cassandra, A. R. Planning and acting in partially observable stochastic domains. *Artificial intelligence*, 101(1-2):99–134, 1998.

Kingma, D. P. and Ba, J. Adam: A method for stochastic optimization. *arXiv preprint arXiv:1412.6980*, 2014.

Laskin, M., Lee, K., Stooke, A., Pinto, L., Abbeel, P., and Srinivas, A. Reinforcement learning with augmented data. In *Advances in Neural Information Processing Systems*, 2020a.

Laskin, M., Srinivas, A., and Abbeel, P. Curl: Contrastive unsupervised representations for reinforcement learning. In *International Conference on Machine Learning*, pp. 5639–5650. PMLR, 2020b.

Lee, A. X., Nagabandi, A., Abbeel, P., and Levine, S. Stochastic latent actor-critic: Deep reinforcement learning with a latent variable model. In *Advances in Neural Information Processing Systems*, 2020a.

Lee, K.-H., Fischer, I., Liu, A., Guo, Y., Lee, H., Canny, J., and Guadarrama, S. Predictive information accelerates learning in RL. *arXiv preprint arXiv:2007.12401*, 2020b.

Liu, G., Zhang, C., Zhao, L., Qin, T., Zhu, J., Jian, L., Yu, N., and Liu, T.-Y. Return-based contrastive representation learning for reinforcement learning. In *International Conference on Learning Representations*, 2021.

Liu, H. and Abbeel, P. Aps: Active pretraining with successor features. In *International Conference on Machine Learning*, pp. 6736–6747. PMLR, 2021a.

Liu, H. and Abbeel, P. Behavior from the void: Unsupervised active pre-training. *arXiv preprint arXiv:2103.04551*, 2021b.

Mazoure, B., Tachet des Combes, R., DOAN, T. L., Bachman, P., and Hjelm, R. D. Deep reinforcement and info-max learning. In *Advances in Neural Information Processing Systems*, 2020.

Mnih, V., Kavukcuoglu, K., Silver, D., Graves, A., Antonoglou, I., Wierstra, D., and Riedmiller, M. Playing atari with deep reinforcement learning. *arXiv preprint arXiv:1312.5602*, 2013.

Oord, A. v. d., Li, Y., and Vinyals, O. Representation learning with contrastive predictive coding. *arXiv preprint arXiv:1807.03748*, 2018.

Pathak, D., Krahenbuhl, P., Donahue, J., Darrell, T., and Efros, A. A. Context encoders: Feature learning by inpainting. In *Proceedings of the IEEE conference on computer vision and pattern recognition*, pp. 2536–2544, 2016.

Radford, A., Narasimhan, K., Salimans, T., and Sutskever, I. Improving language understanding by generative pre-training. 2018.

Radford, A., Wu, J., Child, R., Luan, D., Amodei, D., Sutskever, I., et al. Language models are unsupervised multitask learners. *OpenAI blog*, 1(8):9, 2019.

Schwarzer, M., Anand, A., Goel, R., Hjelm, R. D., Courville, A., and Bachman, P. Data-efficient reinforcement learning with self-predictive representations. In *International Conference on Learning Representations*, 2021a.

Schwarzer, M., Rajkumar, N., Noukhovitch, M., Anand, A., Charlin, L., Hjelm, D., Bachman, P., and Courville, A. Pretraining representations for data-efficient reinforcement learning. *arXiv preprint arXiv:2106.04799*, 2021b.

Shelhamer, E., Mahmoudieh, P., Argus, M., and Darrell, T. Loss is its own reward: Self-supervision for reinforcement learning. *ArXiv*, abs/1612.07307, 2017.

Stooke, A., Lee, K., Abbeel, P., and Laskin, M. Decoupling representation learning from reinforcement learning. *arXiv preprint arXiv:2009.08319*, 2020.

Tassa, Y., Doron, Y., Muldal, A., Erez, T., Li, Y., Casas, D. d. L., Budden, D., Abdolmaleki, A., Merel, J., Lefrancq, A., et al. Deepmind control suite. *arXiv preprint arXiv:1801.00690*, 2018.

Vaswani, A., Shazeer, N., Parmar, N., Uszkoreit, J., Jones, L., Gomez, A. N., Kaiser, Ł., and Polosukhin, I. Attention is all you need. In *Advances in neural information processing systems*, pp. 5998–6008, 2017.

Wei, C., Fan, H., Xie, S., Wu, C.-Y., Yuille, A., and Feichtenhofer, C. Masked feature prediction for self-supervised visual pre-training. *arXiv preprint arXiv:2112.09133*, 2021.

Xie, Z., Zhang, Z., Cao, Y., Lin, Y., Bao, J., Yao, Z., Dai, Q., and Hu, H. Simmim: A simple framework for masked image modeling. *arXiv preprint arXiv:2111.09886*, 2021.

Yarats, D., Zhang, A., Kostrikov, I., Amos, B., Pineau, J., and Fergus, R. Improving sample efficiency in model-free reinforcement learning from images. *arXiv preprint arXiv:1910.01741*, 2019.

Yarats, D., Kostrikov, I., and Fergus, R. Image augmentation is all you need: Regularizing deep reinforcement learning from pixels. In *International Conference on Learning Representations*, 2021.

Ye, W., Liu, S., Kurutach, T., Abbeel, P., and Gao, Y. Mastering atari games with limited data. *Advances in Neural Information Processing Systems*, 34, 2021.

Yu, T., Lan, C., Zeng, W., Feng, M., Zhang, Z., and Chen, Z. Playvirtual: Augmenting cycle-consistent virtual trajectories for reinforcement learning. In Beygelzimer, A., Dauphin, Y., Liang, P., and Vaughan, J. W. (eds.), *Advances in Neural Information Processing Systems*, 2021. URL <https://openreview.net/forum?id=InYbKA26YG2>.

Zhang, A., McAllister, R. T., Calandra, R., Gal, Y., and Levine, S. Learning invariant representations for reinforcement learning without reconstruction. In *International Conference on Learning Representations*, 2021.

Zhu, J., Xia, Y., Wu, L., Deng, J., Zhou, W., Qin, T., and Li, H. Masked contrastive representation learning for reinforcement learning. *arXiv preprint arXiv:2010.07470*, 2020.

Ziebart, B. D., Maas, A. L., Bagnell, J. A., Dey, A. K., et al. Maximum entropy inverse reinforcement learning. In *Aaai*, volume 8, pp. 1433–1438. Chicago, IL, USA, 2008.

Łukasz Kaiser, Babaeizadeh, M., Miłos, P., Osiński, B., Campbell, R. H., Czechowski, K., Erhan, D., Finn, C., Kozakowski, P., Levine, S., Mohiuddin, A., Sepassi, R., Tucker, G., and Michalewski, H. Model based reinforcement learning for atari. In *International Conference on Learning Representations*, 2020.

A. Extended Background of Soft Actor-Critic

Soft Actor-Critic (SAC) (Haarnoja et al., 2018) is an off-policy actor-critic style algorithm. SAC is based on a maximum entropy RL framework where the standard maximum reward RL objective is augmented with an entropy maximization term (Ziebart et al., 2008). SAC has a soft Q-function Q and a policy π .

The soft Q-function is learned by minimizing the soft Bellman error:

$$J(Q) = \mathbb{E}_{tr \sim \mathcal{D}}[(Q(\mathbf{s}_t, \mathbf{a}_t) - (r_t + \gamma \bar{V}(\mathbf{s}_{t+1})))^2], \quad (7)$$

where $tr = (\mathbf{s}_t, \mathbf{a}_t, r_t, \mathbf{s}_{t+1})$ is a tuple with current state \mathbf{s}_t , action \mathbf{a}_t , successor \mathbf{s}_{t+1} and reward r_t , \mathcal{D} is the replay buffer and \bar{V} is the target value function. \bar{V} has the following expectation:

$$\bar{V}(\mathbf{s}_t) = \mathbb{E}_{\mathbf{a}_t \sim \pi}[\bar{Q}(\mathbf{s}_t, \mathbf{a}_t) - \alpha \log \pi(\mathbf{a}_t | \mathbf{s}_t)], \quad (8)$$

where \bar{Q} is the target Q-function whose parameters are updated by an exponentially moving average of the parameters of the Q-function Q , and the temperature α is used to balance the return maximization and the entropy maximization.

The policy π is represented by using reparameterization trick and optimized by minimizing the following objective:

$$J(\pi) = \mathbb{E}_{\mathbf{s}_t \sim \mathcal{D}, \epsilon_t \sim \mathcal{N}}[\alpha \log \pi(f_\pi(\epsilon_t; \mathbf{s}_t) | \mathbf{s}_t) - Q(\mathbf{s}_t, f_\pi(\epsilon_t; \mathbf{s}_t))], \quad (9)$$

where ϵ_t is the input noise vector sampled from Gaussian distribution $\mathcal{N}(0, I)$, and $f_\pi(\epsilon_t; \mathbf{s}_t)$ denotes actions sampled stochastically from the policy π , *i.e.*, $f_\pi(\epsilon_t; \mathbf{s}_t) \sim \tanh(\mu_\pi(\mathbf{s}_t) + \sigma_\pi(\mathbf{s}_t) \odot \epsilon_t)$.

B. Implementation Detail

B.1. Network Architecture

Our model has two parts: the basic networks and the auxiliary networks. The basic networks consist of a representation network (*i.e.*, encoder) f parameterized by θ_f and the policy learning networks of SAC (Haarnoja et al., 2018) ω parameterized by θ_ω .

We follow CURL (Laskin et al., 2020b) to build the architecture of the basic networks. The encoder is composed of 4 convolutional layers (with a rectified linear units (ReLU) activation after each), a fully connected (FC) layer and an layer normalization (LN) (Ba et al., 2016) layer. And the policy learning networks are built by multilayer perceptrons (MLP).

Table 6. Number of parameters of main networks in MLR.

Network	Encoder	Predictive Latent Decoder	Projection Head	Prediction Head
Param.	4.04M	40.8K	10.2K	10.2K

Our auxiliary networks have online networks and momentum (or target) networks. The online networks consist of an encoder f , a predictive latent decoder (PLD) ϕ , a projection head g and a prediction head q , parameterized by θ_f , θ_ϕ , θ_g and θ_q , respectively. Notably, the encoders in the basic networks and the auxiliary networks are *shared*. As shown in Figure 1, there are a momentum encoder \bar{f} and a momentum projection head \bar{g} for computing the self-supervised targets. The momentum networks have the same architectures as the corresponding online networks. Our PLD is a transformer encoder (Vaswani et al., 2017) and has two standard attention layers (with a single attention head). We use an FC layer as the action embedding head to transform the original action to an embedding which has the same dimension of the state representation (*i.e.*, state token). We use sine and cosine functions to build the positional embedding following (Vaswani et al., 2017):

$$p_{(pos, 2j)} = \sin(pos/10000^{2j/d}), \quad (10)$$

$$p_{(pos, 2j+1)} = \cos(pos/10000^{2j/d}), \quad (11)$$

where pos is the position, j is the dimension and d is the embedding size (equal to the state representation size). Both the projection head and the prediction head have two FC layers with a hidden size of 100 and a ReLU activation is followed by the first FC layer. We further present the parameters of the main networks in our method in Table 6. The encoder dominates the number of parameters in the auxiliary networks, which implies that the encoder plays a major role in the masked prediction.

Algorithm 1 Training Algorithm for MLR

Require: An online encoder f , a momentum encoder \bar{f} , a predictive latent decoder ϕ , an online projection head g , a momentum projection head \bar{g} , a prediction head q and policy learning networks ω , parameterized by $\theta_f, \bar{\theta}_f, \theta_\phi, \theta_g, \bar{\theta}_g, \theta_q$ and θ_ω , respectively; a stochastic cube masking function $Mask(\cdot)$; a stochastic image augmentation function $Aug(\cdot)$. Determine auxiliary loss weight λ , sequence length K , mask ratio η , cube size $h \times w \times k$ and EMA coefficient m . Initialize a replay buffer \mathcal{D} . Initialize $Mask(\cdot)$ with η and $h \times w \times k$. Initialize all network parameters.

while train **do**

- Interact with the environment based on the policy
- Collect the transition: $\mathcal{D} \leftarrow \mathcal{D} \cup (\mathbf{o}, \mathbf{a}, \mathbf{o}_{next}, r)$
- Sample a trajectory of K timesteps from \mathcal{D} : $\{\mathbf{o}_t, \mathbf{a}_t, \mathbf{o}_{t+1}, \mathbf{a}_{t+1}, \dots, \mathbf{o}_{t+K-1}, \mathbf{a}_{t+K-1}\}$
- $\mathcal{L}_{mlr} \leftarrow 0; \mathcal{L}_{rl} \leftarrow 0$
- Randomly mask the observation sequence: $\{\tilde{\mathbf{o}}_t, \tilde{\mathbf{o}}_{t+1}, \dots, \tilde{\mathbf{o}}_{t+K-1}\} \leftarrow Mask(\{\mathbf{o}_t, \mathbf{o}_{t+1}, \dots, \mathbf{o}_{t+K-1}\})$
- Perform encoding: $\{\tilde{\mathbf{s}}_t, \tilde{\mathbf{s}}_{t+1}, \dots, \tilde{\mathbf{s}}_{t+K-1}\} \leftarrow \{f(Aug(\tilde{\mathbf{o}}_t)), f(Aug(\tilde{\mathbf{o}}_{t+1})), \dots, f(Aug(\tilde{\mathbf{o}}_{t+K-1}))\}$
- Perform decoding: $\{\hat{\mathbf{s}}_t, \hat{\mathbf{s}}_{t+1}, \dots, \hat{\mathbf{s}}_{t+K-1}\} \leftarrow \phi(\{\tilde{\mathbf{s}}_t, \tilde{\mathbf{s}}_{t+1}, \dots, \tilde{\mathbf{s}}_{t+K-1}\}; \{\mathbf{a}_t, \mathbf{a}_{t+1}, \dots, \mathbf{a}_{t+K-1}\})$
- Perform project and prediction: $\{\hat{\mathbf{y}}_t, \hat{\mathbf{y}}_{t+1}, \dots, \hat{\mathbf{y}}_{t+K-1}\} \leftarrow \{q(g(\hat{\mathbf{s}}_t)), q(g(\hat{\mathbf{s}}_{t+1})), \dots, q(g(\hat{\mathbf{s}}_{t+K-1}))\}$
- Calculate targets: $\{\bar{\mathbf{y}}_t, \bar{\mathbf{y}}_{t+1}, \dots, \bar{\mathbf{y}}_{t+K-1}\} \leftarrow \{\bar{g}(\bar{f}(Aug(\mathbf{o}_t))), \bar{g}(\bar{f}(Aug(\mathbf{o}_{t+1}))), \dots, \bar{g}(\bar{f}(Aug(\mathbf{o}_{t+K-1})))\}$
- Calculate MLR loss: $\mathcal{L}_{mlr} \leftarrow 2 - \frac{2}{K} \sum_{i=0}^{K-1} \frac{\|\hat{\mathbf{y}}_{t+i}\|_2}{\|\tilde{\mathbf{y}}_{t+i}\|_2} \frac{\|\bar{\mathbf{y}}_{t+i}\|_2}{\|\tilde{\mathbf{y}}_{t+i}\|_2}$
- Calculate RL loss \mathcal{L}_{rl} based on a given base RL algorithm (*e.g.*, SAC)
- $\mathcal{L}_{total} \leftarrow \mathcal{L}_{rl} + \lambda \mathcal{L}_{mlr}$
- $(\theta_f, \theta_\phi, \theta_g, \theta_q, \theta_\omega) \leftarrow Optimize((\theta_f, \theta_\phi, \theta_g, \theta_q, \theta_\omega), \mathcal{L}_{total})$
- $(\bar{\theta}_f, \bar{\theta}_g) \leftarrow m(\bar{\theta}_f, \bar{\theta}_g) + (1 - m)(\theta_f, \theta_g)$

end while

B.2. Training Detail

Optimization. The training algorithm of our method is presented in Algorithm 1. We use Adam optimizer (Kingma & Ba, 2014) to optimize all parameters in our model, with $(\beta_1, \beta_2) = (0.9, 0.999)$ (except for $(0.5, 0.999)$ for SAC temperature α). Following (Vaswani et al., 2017), we warmup the learning rate of our MLR objective by

$$lr = lr_0 \cdot \min(step_num^{-0.5}, step_num \cdot warmup_step^{-1.5}), \quad (12)$$

where the lr and lr_0 denote the current learning rate and the initial learning rate, respectively, and $step_num$ and $warmup_step$ denote the current step and the warmup step, respectively. In this work, we run each model by using a single NVIDIA Tesla V100 GPU.

Date augmentation. Modest data augmentation such as crop or shift is shown to be effective for improving RL agent performance in vision-based RL (Yarats et al., 2021; Laskin et al., 2020a; Schwarzer et al., 2021a; Yu et al., 2021). Following PlayVirtual (Yu et al., 2021), we perform random crop on the observations in training the RL objective \mathcal{L}_{rl} and random crop and intensity in training the auxiliary objective, *i.e.*, \mathcal{L}_{mlr} .

B.3. Hyperparameters.

We list the hyperparameters used for DMControl benchmarks (Tassa et al., 2018) in Table 8.

C. Extended Ablation Study

Sequence length. Table shows the results of the observation sequence length K at $\{8, 16, 24\}$. A large K (*e.g.*, 24) does not bring further performance improvement as the network can reconstruct the missing content in a trivial way like copying and pasting the missing content from other states, while a small K like 8 may not be sufficient for learning rich context information. 16 is a good trade-off in our experiment.

Cube size. Our space-time cube can be flexibly designed. We ablate the influence of the spatial size (h and w , $h = w$ by default) and temporal depth k , as shown in Figure 6a and 6b. In general, a proper cube size leads to good results. The spatial

Table 7. Ablation study of sequence length K . We run each model on DMControl-100k benchmark with 5 random seeds.

Env.	Baseline	K=8	K=16	K=24
Fing.spin	822 ± 146	816 ± 129	907 ± 69	875 ± 63
Cart.swin	782 ± 74	857 ± 3	791 ± 50	781 ± 58
Reac.easy	557 ± 137	779 ± 116	875 ± 92	736 ± 247
Chee.run	438 ± 33	469 ± 51	495 ± 13	454 ± 41
Walk.walk	414 ± 310	473 ± 264	597 ± 102	533 ± 98
Ball.catch	669 ± 310	910 ± 58	939 ± 9	944 ± 22
Mean	613.7	717.3	767.3	720.5
Median	613.0	797.5	833.0	758.5

size has a large influence on the final performance. A moderate spatial size 10×10 is good for MLR. The performance generally has a upward tendency when increasing the cube depth k . However, a cube mask with too large k (e.g., 16) possibly masks some necessary contents for the reconstruction and hinders the training.

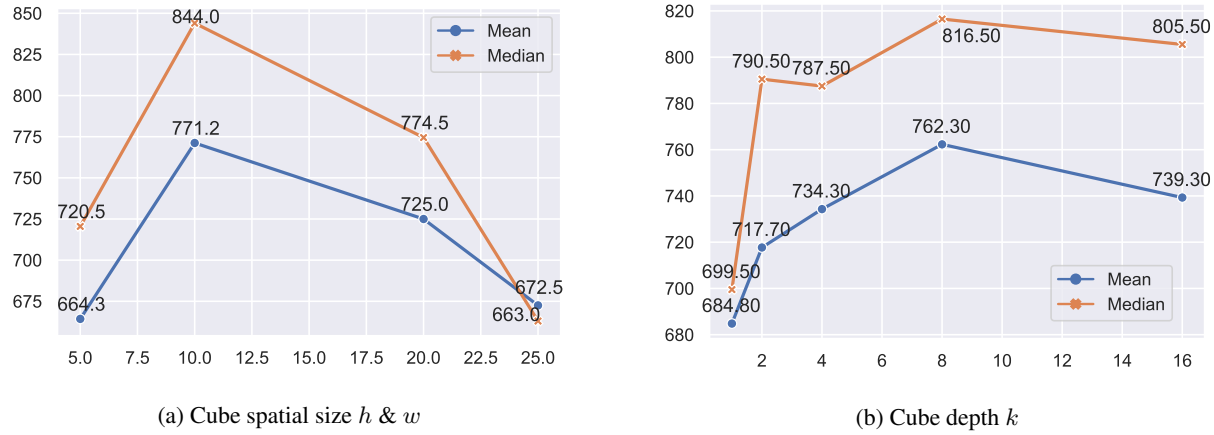


Figure 6. Ablation studies of (a) cube spatial size h & w and (b) cube depth k . We report the mean and median scores on DMControl-100k benchmark. The result of each model is averaged over 3 random seeds.

Table 8. Hyperparameters used for DMControl environments.

Hyperparameter	Value
Frame stack	3
Observation rendering	(100, 100)
Observation downsampling	(84, 84)
Augmentation for policy learning	Random crop
Augmentation for auxiliary task	Random crop and intensity
Replay buffer size	100000
Initial exploration steps	1000
Action repeat	2 <i>Finger, spin</i> and <i>Walker, walk</i> ; 8 <i>Cartpole, swingup</i> ; 4 otherwise
Evaluation episodes	10
Optimizer	Adam
$(\beta_1, \beta_2) \rightarrow (\theta_f, \theta_\phi, \theta_g, \theta_q, \theta_\omega)$	(0.9, 0.999)
$(\beta_1, \beta_2) \rightarrow (\alpha)$ (temperature in SAC)	(0.5, 0.999)
Learning rate $(\theta_f, \theta_\omega)$	0.0002 <i>Cheetah, run</i> 0.001 otherwise
Learning rate $(\theta_f, \theta_\phi, \theta_g, \theta_q)$	0.0001 <i>Cheetah, run</i> 0.0005 otherwise
Learning rate warmup $(\theta_f, \theta_\phi, \theta_g, \theta_q)$	6000 steps
Learning rate (α)	0.0001
Batch size for policy learning	512
Batch size for auxiliary task	128
Q-function EMA m	0.99
Critic target update freq	2
Discount factor	0.99
Initial temperature	0.1
Target network update period	1
Target network EMA m	0.9 <i>Walker, walk</i> 0.95 otherwise
State representation dimension d	50
Important Hyperparameters in MLR	
Weight of MLR loss λ	1
Mask ratio η	50%
Sequence length K	16
Cube spatial size $h \times w$	10×10
Cube depth k	4 <i>Cartpole, swingup</i> and <i>Reacher, easy</i> 8 otherwise
Decoder depth L (number of attention layers)	2